

# An Analytic Approach to the CMB Polarization Generated by Relic Gravitational Waves

Wen Zhao and Yang Zhang

Astrophysics Center

University of Science and Technology of China

Hefei, Anhui, China

## Abstract

We develop Polnarev's analytic method to calculate of the polarization power spectrum of the cosmic microwave background radiation (CMB) generated by cosmic relic gravitational waves. In this analytic approach the physics involved in this process is more transparent. Consequently, the effects due to various elements of physics can be isolated easily. In numerically calculating the evolution of the gravitational waves during the radiation-matter transition, the WKB approximation for the scale factor has been taken. To describe more precisely the decoupling process, we have introduced an analytic expression for the visibility function, consisting of two pieces of half-gaussian curves. We also include the damping effects on the power spectrum at small scale up to the second order of the tight coupling due to the collisions. An analytic polarization spectra  $C_l^{XX}$  has been obtained with following several improvements over the previous results. 1. The approximate analytic result is quite close to the numerical one evaluated from the cmbfast code, especially, for the first three peaks of the spectrum that are observable. By using the analytic exact solution of relic gravitational waves from the sudden-change approximation, we have demonstrated the dependence of  $C_l^{XX}$  on the dark energy and the baryon. 2. Our analytic half-gaussian approximation of the visibility function fits analytically better than the usual Gaussian model, and its time integration yields a parameter-dependent damping factor. This improves the spectrum  $\Delta C_l^{XX}/C_l^{XX} \sim 30\%$  around the second and third peaks. 3. The second order of tight coupling limit reduces the amplitude of  $C_l^{XX}$  by 58%, comparing with the first order. 4. The influence of the power spectrum index of relic GW is such that a larger value of  $n_T$  produces higher polarization spectra  $C_l^{XX}$ .

PACS numbers: 98.80.-k, 98.80.Es, 04.30.-w, 04.62+v,

Key words: gravitational waves, cosmic microwave background radiation, polarization

e-mail: yzh@ustc.edu.cn

## 1. Introduction.

Studies on the anisotropy and polarization of CMB have made great progress, yielding important information of cosmology. Recently, Wilkinson Microwave Anisotropy Probe (WMAP) observational results on the CMB anisotropy and polarization power spectrums [1, 2, 3, 4, 5, 6] agree well with the prediction of inflation of a spatially flat Universe with the nearly scale-invariant and Gaussian spectrum of primordial adiabatic perturbations. Inflationary expansion can generate two type of perturbations  $h_{ij}$  of spacetime metric: one is the scalar type (density) of perturbations [7, 8, 9], and the other is the tensorial type (relic gravitational waves) [10, 11, 12, 13, 14, 7, 9]. These two kinds of perturbations will enter the Boltzmann equation for photons and influence CMB during the decoupling. Their impact on the anisotropy and polarization of CMB are different, especially their respective contributions are not completely determined theoretically. The major contribution to CMB anisotropies and polarization are from the density perturbations [15, 16]. However, the tensorial contribution is also important, especially in long wave-length range. Moreover, the magnetic type of polarization of CMB can only be generated by the tensorial perturbations, and it thus provides another channel to detect the relic gravitational waves besides the direct detection of laser interferometer [17, 18, 19, 20].

The power spectra of CMB polarization can be calculated by numerical method [21, 22], which gives rather precise predictions. But the semi-analytic method is also very helpful in analyzing the underlying physics and in revealing the dependence on the cosmological parameters [23]. A common treatment uses the spherical harmonic functions to expand the Boltzmann equation into a hierarchical set of equations for the multipole moments, then solves each of them separately [21, 24, 25, 26]. The other treatment was first suggested by Polnarev [14], using a basis of polarization vectors to decompose the Boltzmann equation, ending up with only two equations for the two unknown distribution functions,  $\zeta$  and  $\beta$ , standing for the anisotropy and the polarization, respectively. This treatment is simpler and has been further used [27, 28, 29, 30, 31, 32, 33]. In this paper, we study the CMB polarization caused by the relic gravitational waves in the Polnarev framework. Our result is an analytic formula of the polarization power spectrum, which depends explicitly on the visibility function and on the spectrum of the relic gravitational waves at the decoupling. In our treatment for the ionization history through recombination we use a half-gaussian visibility function, which is more precise than the usual gaussian function. For the relic gravitational waves we use a WKB approximation. When doing integration for the Boltzmann equations, we find there are two kind of damping mechanism on the power spectrum: one is caused by the visibility function, which causes damping at small scale, and another is the second order tight coupling limit when solving the Boltzmann equations, which is only a simple factor damping in all scale. The latter is different from the case of the scalar perturbation sources, where the so-called "silk damping", which only causes the damping for the power spectrum at the small scale. We also find that the final power spectra depend sensitively on the state of tensor perturbations at the decoupling time (the ratio of the positive and negative modes), which is complex and prevents us from getting an exact formula for the power spectrums.

The organization of this paper is as follows: in Section 2 and 3, we write down the evolution equations of the polarization distribution function  $\beta_l$ , and the exact relations of  $C_l^{GG}$  and  $C_l^{CC}$  with it. For the following discussion, we calculate the evolution of the gravitational waves and build the visibility function models in Section 4 and 5. In Section 6, we have an approximately analytic calculation of the Boltzmann equations, and give the expression of  $\beta_l$ , which follows the expression of the power spectrum functions  $C_l^{GG}$  and  $C_l^{CC}$ . At last, we give a conclusion and discussion in Section 7, where we main discuss the effect of tensor-scalar ratio  $r$ , the baryon

density  $\Omega_b$ , dark energy density  $\Omega_\Lambda$  and the reionization process on the power spectrums.

## 2. CMB Polarization.

The polarized distribution function of photons is generally represented by a column vector  $f = (I_l, I_r, U, V)$ , and its components are related to the Stokes parameters:  $I = I_l + I_r$  and  $Q = I_l - I_r$ . An important property of the Stokes parameters is that, under a rotation  $\delta$  about the axis of propagation, the total intensity  $I$  and the parameter  $V$  are invariant, but  $Q$  and  $U$  transform as [34]

$$\begin{pmatrix} Q' \\ U' \end{pmatrix} = \begin{pmatrix} \cos 2\delta & \sin 2\delta \\ -\sin 2\delta & \cos 2\delta \end{pmatrix} \begin{pmatrix} Q \\ U \end{pmatrix}.$$

So  $(Q, U)$  together form a spin-2 field according to the coordinate transformation, and can be conveniently described by a  $2 \times 2$  polarization tensor. For actual detections the photon come from the full sky of 2-sphere, which in the spherical coordinates  $(\theta, \phi)$  has a metric

$$g_{ab} = \begin{pmatrix} 1 & 0 \\ 0 & \sin^2 \theta \end{pmatrix}, \quad (1)$$

the polarization tensor is [30]

$$P_{ab}(\hat{n}) = \frac{1}{2} \begin{pmatrix} Q(\hat{n}) & -U(\hat{n}) \sin \theta \\ -U(\hat{n}) \sin \theta & Q(\hat{n}) \sin^2 \theta \end{pmatrix}, \quad (2)$$

satisfying  $P_{ab} = P_{ba}$ , and  $g^{ab}P_{ab} = 0$ .

During the era prior to the decoupling in the early Universe, the Thompson scattering of anisotropic radiation by free electrons can give rise to the linear polarization only, and does not generate the circular polarization  $V$ , so we only consider  $f = (I_l, I_r, U)$ . For the trivial case of a homogeneous and isotropic unpolarized radiation, the distribution is simply  $f = f_0(\nu)(1, 1, 0)$ , where  $f_0(\nu) = \frac{1}{e^{h\nu/kT} - 1}$  is the usual blackbody distribution function with temperature  $T$ . The combined effects of the Thompson scattering and the metric perturbations will yield linear polarizations of photons. The time evolution of the photon distribution function is determined by the equation of radiative transfer, essentially the Boltzmann equation [34],

$$\frac{\partial f}{\partial \eta} + \hat{n}^i \frac{\partial f}{\partial x^i} = -\frac{d\nu}{d\eta} \frac{\partial f}{\partial \nu} - q(f - J), \quad (3)$$

where  $\hat{n}^i$  is the unit vector in the direction  $(\theta, \phi)$  of photon propagation,  $q = \sigma_T n_e a$  is the differential optical depth and has the meaning of scattering rate,  $\sigma_T = 6.65 \times 10^{-25} \text{cm}^2$  is the Thompson cross-section,  $n_e$  is the number density of the free electron, and

$$J = \frac{1}{4\pi} \int_{-1}^1 d\mu' \int_0^{2\pi} d\phi' P(\mu, \phi, \mu', \phi') f(\eta, x^i, \nu, \mu', \phi'), \quad (4)$$

where  $\mu = \cos \theta$ ,  $\mu' = \cos \theta'$  and

$$P = \begin{pmatrix} \mu^2 \mu'^2 \cos 2(\phi' - \phi) & -\mu^2 \cos 2(\phi' - \phi) & \mu^2 \mu' \sin 2(\phi' - \phi) \\ -\mu^2 \cos 2(\phi' - \phi) & \cos 2(\phi' - \phi) & -\mu \sin 2(\phi' - \phi) \\ -2\mu \mu'^2 \sin 2(\phi' - \phi) & 2\mu \sin 2(\phi' - \phi) & 2\mu \mu' \cos 2(\phi' - \phi) \end{pmatrix} \quad (5)$$

is the phase-matrix. The scattering term  $q(f-J)$  in Eq.(3) describes the effect of the Thompson scattering by free electrons, and the term  $-\frac{d\nu}{d\eta}\frac{\partial f}{\partial \nu}$  reflects the effect of variation of frequency due to the metric perturbations through the Sachs-Wolfe formula [35]

$$\frac{1}{\nu} \frac{d\nu}{d\eta} = \frac{1}{2} \frac{\partial h_{ij}}{\partial \eta} \hat{n}^i \hat{n}^j.$$

In the presence of perturbations  $h_{ij}$ , either scalar or tensorial, the distribution function will be perturbed and can be generally written as

$$f(\theta, \phi) = f_0 \left[ \begin{pmatrix} 1 \\ 1 \\ 0 \end{pmatrix} + f_1 \right], \quad (6)$$

where  $f_1$  represents the perturbed portion.

The perturbed flat Robertson-Walker (FRW) metric is

$$ds^2 = a^2(\eta) \left[ d\eta^2 - (\delta_{ij} + h_{ij}) dx^i dx^j \right]. \quad (7)$$

where  $\eta = \int (a_0/a) dt$  is the conformal time, and  $h_{ij}$  are the perturbations with  $|h_{ij}| \ll 1$ . In our context, we consider only the tensorial type perturbations  $h_{ij}$ , representing the relic gravitational waves. So they are symmetric  $h_{ij} = h_{ji}$ , traceless  $h_{ii} = 0$ , and transverse  $h_{ij,j} = 0$ . Therefore, there are only two independent modes, corresponding to the  $+$  and  $\times$  gravitational-wave polarizations.

$$h_{ij} = h_{ij}^+ + h_{ij}^\times = h^+ \epsilon_{ij}^+ + h^\times \epsilon_{ij}^\times.$$

Taking the direction of propagation of the GW in the direction of  $\hat{z}$ ,  $\hat{k} = \hat{z}$ , then the polarization tensors for the GW satisfy

$$\epsilon_{ij}^+ \hat{n}_i \hat{n}_j = \sin^2 \theta \cos 2\phi, \quad \epsilon_{ij}^\times \hat{n}_i \hat{n}_j = \sin^2 \theta \sin 2\phi.$$

In cosmological context, it is usually assumed that the two components  $h^+$  and  $h^\times$  have the same magnitude and are of the same statistical properties. To simplify the Boltzmann equation (3), for the  $h_{ij} = h^+ \epsilon_{ij}^+$  polarization, one writes the perturbed distribution function  $f_1$  in the form [14]

$$f_1 = \frac{\zeta}{2} (1 - \mu^2) \cos 2\phi \begin{pmatrix} 1 \\ 1 \\ 0 \end{pmatrix} + \frac{\beta}{2} \begin{pmatrix} (1 + \mu^2) \cos 2\phi \\ -(1 + \mu^2) \cos 2\phi \\ 4\mu \sin 2\phi \end{pmatrix}. \quad (8)$$

For the  $h_{ij} = h^\times \epsilon_{ij}^\times$  polarization, one writes  $f_1$  in the form

$$f_1 = \frac{\zeta}{2} (1 - \mu^2) \sin 2\phi \begin{pmatrix} 1 \\ 1 \\ 0 \end{pmatrix} + \frac{\beta}{2} \begin{pmatrix} (1 + \mu^2) \sin 2\phi \\ -(1 + \mu^2) \sin 2\phi \\ -4\mu \cos 2\phi \end{pmatrix}, \quad (9)$$

where  $\zeta$  represents the anisotropy of photon distribution since  $\zeta \propto I_l + I_r = I$ , and  $\beta$  represents the polarization of photons since  $\beta \propto I_l - I_r = Q$ . Both  $\zeta$  and  $\beta$  are to be determined by solving the Boltzmann equation. For the  $h_{ij} = h^+ \epsilon_{ij}^+$  polarization, one substitutes  $f$  into Eq.(3). Upon taking Fourier transformation, retaining only the terms linear in the perturbation  $h_{ij}$ , and performing the integration over  $d\mu$ , one arrives at a set of two differential equations [14, 32, 33],

$$\dot{\xi}_k + [ik\mu + q] \xi_k = \frac{d \ln f_0}{d \ln \nu_0} \dot{h}_k^+, \quad (10)$$

$$\dot{\beta}_k + [ik\mu + q] \beta_k = \frac{3}{16} q \int d\mu' \left[ (1 + \mu'^2)^2 \beta_k - \frac{1}{2} (1 - \mu'^2)^2 \xi_k \right]. \quad (11)$$

For the  $h_{ij} = h^\times \epsilon_{ij}^\times$  polarization, the resulting equations are the same as Eqs.(10) and (11) with  $\dot{h}^+$  being replaced by  $\dot{h}^\times$ . In Eq.(10) and (11)  $\xi_k \equiv \zeta_k + \beta_k$ ,  $k$  is the wavenumber,  $\xi_k$ ,  $\beta_k$ , and  $h_k^+$  are the Fourier modes of  $\xi$ ,  $\beta$ , and  $h^+$ , respectively, and the over dot “.” denotes  $d/d\eta$ . In the following, for simplicity, we will omit the sub-index  $k$  of the function  $\xi_k$ ,  $\beta_k$  and  $h_k$ . Moreover, we also drop the GW polarization notation,  $+$  or  $\times$ , since both  $h^+$  and  $h^\times$  are similar in computations. From the structure of Eqs.(10) and (11), one can see that the  $\dot{h}$  of GW in Eq.(10) plays the role of a source for the anisotropies  $\xi$ , which in turn plays the role of a source for the polarization  $\beta$  in Eq.(11). Our work is to find the solution of  $\beta$ , then calculate the CMB polarization power spectra.

In the simple case of the long-wavelength limit with  $k = 0$ , this set of equations reduces to

$$\dot{\xi} + q\xi = \dot{h}, \quad (12)$$

$$\dot{\beta} + \frac{3}{10} q\beta = -\frac{1}{10} q\xi. \quad (13)$$

The solutions  $\beta$  and  $\xi$  will be independent of the angle  $\mu$ . In general case of  $k \neq 0$ , the function  $\beta$  and  $\xi$  to be determined by Eqs.(10) and (11) will depend on  $\mu$ . As the right hand side of Eq.(11) contains an integral over  $d\mu'$ , it is difficult to give an exact solution. And one may expand  $\beta$  and  $\xi$  in terms of the Legendre functions

$$\xi(\mu) = \sum_l (2l+1) \xi_l P_l(\mu),$$

$$\beta(\mu) = \sum_l (2l+1) \beta_l P_l(\mu),$$

with the Legendre components

$$\xi_l(\eta) = \frac{1}{2} \int_{-1}^1 d\mu \xi(\eta, \mu) P_l(\mu), \quad (14)$$

$$\beta_l(\eta) = \frac{1}{2} \int_{-1}^1 d\mu \beta(\eta, \mu) P_l(\mu). \quad (15)$$

The differential equations Eqs.(10) and (11) for  $\xi(\eta, \mu)$  and  $\beta(\eta, \mu)$  then become an infinite set of coupled differential equations for  $\xi_l(\eta)$  and  $\beta_l(\eta)$ .

### 3. Decomposition of Polarization $\beta$ into Electric and Magnetic Types

From Eq.(8) for the definition of  $\zeta$  and  $\beta$  for the  $h^+$  GW polarization, it is seen that the Stokes parameters can be written as the following [30, 32],

$$Q(\theta, \phi) = \frac{T_0}{4} \sum_l (2l+1) P_l(\cos \theta) (1 + \cos^2 \theta) \cos 2\phi \beta_l; \quad (16)$$

$$U(\theta, \phi) = \frac{T_0}{4} \sum_l (2l+1) P_l(\cos \theta) 2 \cos \theta \sin 2\phi \beta_l. \quad (17)$$

One commonly uses the spherical harmonic functions  $Y_{lm}$  as the complete orthonormal basis for scalar functions defined on the 2-sphere, such as the temperature anisotropies  $\Delta T$ . For the

$2 \times 2$  tensors defined on the 2-sphere, such as  $P_{ab}$  in Eq.(2), the following complete orthonormal set of tensor spherical harmonics can be employed [30]:

$$Y_{(lm)ab}^G = N_l \left( Y_{(lm):ab} - \frac{1}{2} g_{ab} Y_{(lm):c}^c \right), \quad (18)$$

$$Y_{(lm)ab}^C = \frac{N_l}{2} \left( Y_{(lm):ac} \epsilon^c_b + Y_{(lm):bc} \epsilon^c_a \right), \quad (19)$$

where “:” denotes covariant derivative on the 2-sphere,  $N_l \equiv \sqrt{2(l-2)!/(l+2)!}$ , and

$$\epsilon^a_b = \begin{pmatrix} 0 & \sin \theta \\ -1/\sin \theta & 0 \end{pmatrix}. \quad (20)$$

They satisfy

$$\int d\hat{n} Y_{(lm)ab}^{G*}(\hat{n}) Y_{(l'm')ab}^G(\hat{n}) = \int d\hat{n} Y_{(lm)ab}^{C*}(\hat{n}) Y_{(l'm')ab}^C(\hat{n}) = \delta_{ll'} \delta_{mm'}, \quad (21)$$

$$\int d\hat{n} Y_{(lm)ab}^{G*}(\hat{n}) Y_{(l'm')ab}^C(\hat{n}) = 0. \quad (22)$$

By construction one sees that  $Y_{(lm)ab}^G$  is the gradients (electric type) and  $Y_{(lm)ab}^C$  is the curls (magnetic type) of the ordinary spherical harmonics, and they represent the electric type and magnetic type components of the polarization, respectively. The polarization tensor can be expanded in terms of this basis as:

$$\frac{P_{ab}(\hat{n})}{T_0} = \sum_{l=2}^{\infty} \sum_{m=-l}^l \left[ a_{(lm)}^G Y_{(lm)ab}^G(\hat{n}) + a_{(lm)}^C Y_{(lm)ab}^C(\hat{n}) \right]. \quad (23)$$

The expansion coefficients are given by

$$a_{(lm)}^G = \frac{1}{T_0} \int d\hat{n} P_{ab}(\hat{n}) Y_{(lm)ab}^{G*}(\hat{n}), \quad a_{(lm)}^C = \frac{1}{T_0} \int d\hat{n} P_{ab}(\hat{n}) Y_{(lm)ab}^{C*}(\hat{n}), \quad (24)$$

and calculation yields [30, 32]:<sup>1</sup>

$$a_{lm}^G = \frac{1}{8} (\delta_{m2} + \delta_{m,-2}) \sqrt{2\pi(2l+1)} \times \left[ \frac{(l+2)(l+1)\beta_{l-2}}{(2l-1)(2l+1)} + \frac{6(l-1)(l+2)\beta_l}{(2l+3)(2l-1)} + \frac{l(l-1)\beta_{l+2}}{(2l+3)(2l+1)} \right], \quad (25)$$

$$a_{lm}^C = \frac{-i}{4} \sqrt{\frac{2\pi}{(2l+1)}} (\delta_{m2} - \delta_{m,-2}) [(l+2)\beta_{l-1} + (l-1)\beta_{l+1}]. \quad (26)$$

where the polarization  $\beta$  shows up explicitly in the G and C components. Then the magnetic type of power spectrum  $C_l^{GG}$  is<sup>2</sup>

$$\begin{aligned} C_l^{GG} &= \frac{1}{2l+1} \sum_m |a_{lm}^G|^2 \\ &= \frac{\pi}{16} \left| \frac{(l+2)(l+1)\beta_{l-2}}{(2l-1)(2l+1)} + \frac{6(l-1)(l+2)\beta_l}{(2l+3)(2l-1)} + \frac{l(l-1)\beta_{l+2}}{(2l+3)(2l+1)} \right|^2 \end{aligned} \quad (27)$$

<sup>1</sup>There is a small mistake in the formulae (4.39),(4.40),(4.41) and (4.42) in Ref[30] and formulae (111),(114) and (115) in Ref[32], the coefficient of  $\frac{6l(l+1)}{(2l+3)(2l-1)}$  should be replaced by  $\frac{6(l-1)(l+2)}{(2l+3)(2l-1)}$ .

<sup>2</sup>In the Ref.[30, 32], the bracket of [ ] should be replaced by the absolute value sign | |, which is for the values of  $\beta$  may being imaginary numbers.

and similarly for  $C_l^{\text{CC}}$ . Note that these expressions are for the gravitational wave in the  $\hat{z}$  direction with ‘+’ polarization. Summing over all Fourier modes, and over both polarization states, one has the final result

$$C_l^{\text{GG}} = \frac{1}{16\pi} \int \left| \frac{(l+2)(l+1)\beta_{l-2}}{(2l-1)(2l+1)} + \frac{6(l-1)(l+2)\beta_l}{(2l+3)(2l-1)} + \frac{l(l-1)\beta_{l+2}}{(2l+3)(2l+1)} \right|^2 k^2 dk, \quad (28)$$

$$C_l^{\text{CC}} = \frac{1}{4\pi} \int \left| \frac{(l+2)\beta_{l-1}}{2l+1} + \frac{(l-1)\beta_{l+1}}{2l+1} \right|^2 k^2 dk. \quad (29)$$

Note that the cross-correlation power spectrum vanishes

$$C_l^{\text{GC}} = \sum_{m=-l}^{m=l} \frac{a_{lm}^{\text{G}*} a_{lm}^{\text{C}}}{2l+1} = 0, \quad (30)$$

since  $a_{(lm)}^{\text{G}} \propto (\delta_{m,2} + \delta_{m,-2})$ , while  $a_{(lm)}^{\text{C}} \propto (\delta_{m,2} - \delta_{m,-2})$ .

#### 4. Evolution of Gravitational Waves

Now we consider the evolution of the relic GW, which is the source term of the CMB polarization in Eq.(10). For both polarizations, +,  $\times$ , the equation of motion for the relic GW of mode  $k$  is the following:

$$\ddot{h} + 2\frac{\dot{a}}{a}\dot{h} + k^2 h = 0, \quad (31)$$

and the initial condition is taken to be

$$h(\eta = 0) = h(k), \quad \dot{h}(\eta = 0) = 0, \quad (32)$$

with

$$\frac{k^3}{2\pi^2} |h(k)|^2 = P_h(k) = A_T \left( \frac{k}{k_0} \right)^{n_T}, \quad (33)$$

where  $P_h(k)$  is the the primordial power spectrum of GW,  $A_T$  is the amplitude,  $k_0 = 0.05 \text{ Mpc}^{-1}$  is the pivot wavenumber, and  $n_T$  is the the tensor spectrum index. Inflationary models generically predicts  $n_T \approx 0$ , a nearly scale-invariant spectrum. Later we will also see the influence of  $n_T$  on the CMB polarization. We have ignored a suppressing effect on the gravitational waves by the neutrinos free streaming [36, 37], which can slightly bring down the hight of the peak at small scales [26].

The equation (31) depends on the scale factor  $a(\eta)$ , which is determined by the Friedmann equation

$$\dot{a}^2 = H_0^2 \left[ \Omega_r + a\Omega_m + a^4\Omega_\Lambda \right], \quad (34)$$

where  $H_0$  is the present Hubble parameter,  $\Omega_r$ ,  $\Omega_m$ , and  $\Omega_\Lambda$  are the present fractional densities for the radiation (including the photon and neutrino), matter, and dark energy, respectively. Given a set of these densities, one solves Eq.(34) for  $a(\eta)$  numerically. Taking  $\Omega_r = 8.36 \times 10^{-5}$ ,  $\Omega_m = \Omega_b + \Omega_{dm} = 0.044 + 0.226$ ,  $\Omega_\Lambda = 0.73$ , we solve Eq.(34), and substitute the resulting  $a(\eta)$  and  $\dot{a}(\eta)$  into Eq.(31), then the numerical solutions  $h(\eta)$  and  $\dot{h}(\eta)$  are obtained straightforwardly. The resulting  $h(\eta_d)$  and  $\dot{h}(\eta_d)$  at the decoupling time  $\eta_d$  are given as function of  $k$  in Fig.1 and Fig.2, respectively.

Besides the numerical solution, we may use the simple approximations of  $a(\eta)$  transiting between different stages suddenly,

$$a(\eta) = \begin{cases} a_r \eta, & \eta < \eta_e \quad (\text{radiation dominant}), \\ a_m \eta^2, & \eta_e < \eta \leq \eta_E \quad (\text{matter dominant}), \\ a_l \eta^{-1}, & \eta > \eta_E \quad (\Lambda \text{ dominant}) \end{cases} \quad (35)$$

where  $a_r$ ,  $a_m$ , and  $a_l$  are constant numbers, and can be determined by jointing  $a(\eta)$  at  $\eta_e$  and  $\eta_E$ . In the  $\Lambda$ CDM model<sup>3</sup> with  $\Omega_b = 0.044$ ,  $\Omega_{dm} = 0.226$ ,  $\Omega_\Lambda = 0.73$ , taking the redshift  $z_e = 3234$  yields the conformal time  $\eta_e/\eta_0 = 0.007$  (where  $\eta_0$  is the present conformal time), and taking  $z_E = 0.39$  yields  $\eta_E/\eta_0 = 0.894$ , and  $\eta_d/\eta_0 = 0.0195$  is the decoupling time at the redshift  $z_d = 1089$ . Eq.(31) has the analytic solution [38, 25, 39]:

$$h(\eta) = A_0 j_0(k\eta), \quad (\eta < \eta_e), \quad (36)$$

$$h(\eta) = A_0(\eta_e/\eta)[A_1 j_1(k\eta) + A_2 y_1(k\eta)], \quad (\eta_e < \eta \leq \eta_E), \quad (37)$$

with the coefficient

$$A_0 = (A_T k^{n_T-3})^{1/2}, \quad (38)$$

determined by the primordial power spectrum, and

$$A_1 = \frac{3k\eta_e - k\eta_e \cos(2k\eta_e) + 2 \sin(2k\eta_e)}{2k^2\eta_e^2}, \quad (39)$$

$$A_2 = \frac{2 - 2k^2\eta_e^2 - 2 \cos(2k\eta_e) - k\eta_e \sin(2k\eta_e)}{2k^2\eta_e^2}. \quad (40)$$

These  $h(\eta_d)$  and  $\dot{h}(\eta_d)$  are plotted with solid lines in Fig.1 and Fig.2, where the initial normalization  $h(k) = 1$  has been taken. The figures show that the simple approximation is good only in long wavelengths, but it differs from the numerical one considerably in short wavelength ( $k > 10$ ).

As an improvement to (35), one can use the WKB approximation for  $a(\eta)$  [40, 26]. Since we are only interested in the gravitational waves at time  $\eta_d$ , and the dark energy is small and can be omitted at that time, so the scale factor can be approximated by

$$a(\tau) = a_e \tau(\tau + 2), \quad (41)$$

where  $\tau \equiv (\sqrt{2} - 1)\eta/\eta_e$ , and  $a_e$  is determined by  $a_0/a_e = 1 + z_e$ . When  $\tau \ll 2$ ,  $a(\tau) \rightarrow \tau$ , the radiation dominated stage, and when  $\tau \gg 2$ ,  $a \rightarrow \tau^2$ , the matter dominated stage.  $a(\tau)$  transits between these two stages is smooth. Then the evolution of the gravitational waves become

$$h'' + 2\frac{a'}{a}h' + r^2h = 0, \quad (42)$$

where  $r \equiv k\eta_e/(\sqrt{2} - 1)$ , the prime denotes  $d/d\tau$ . This equation has an analytic solution discussed in Ref.[26], which is rather complex. In this paper, we employ Eq.(41) as an approximation of  $a(\eta)$  to find the numerical solution of Eq.(42). The resulting  $h(\eta_d)$  and  $\dot{h}(\eta_d)$  in this WKB approximation are plotted with the dashed lines in Fig.1 and Fig.2, which show that the results are very good when comparing with the numerical ones, and the difference of them  $\ll 1\%$ . The approximation of (41) is simpler than the numerical  $a(\eta)$ , and has better precision than the simple approximation of (35), and will be used to calculate the CMB polarization power spectrum.

---

<sup>3</sup>In all this paper, we choose the present Hubble parameter  $h_0 = 0.72$ .



## 5. The Model of Decoupling History.

Consider the decoupling history of the Universe. Before the decoupling, the ionized baryons are tightly coupled to photons by Thompson scattering. Once the temperature falls below a few eV, it becomes favorable for electrons and ions to recombine to form neutral atoms. As the number of charged particles falls, the mean free path of any given photon increases. Eventually, the mean free path becomes comparable to the horizon size and the photon and baryon fluids are essentially decoupled, and the CMB photons last scatter. One can solve the ionization equations during the recombination stage to obtain the visibility function  $V(\eta)$ , which describes the probability that a given photon last scattered from a particular time [41, 42], depending on the cosmological parameters, especially  $\Omega_b$  and the present Hubble parameter  $H_0$  [23]. In terms of the optical depth  $\kappa$ , this visibility function is given by

$$V(\eta) = q(\eta)e^{-\kappa(\eta_0, \eta)}, \quad (43)$$

satisfying

$$\int_0^{\eta_0} V(\eta) d\eta = 1, \quad (44)$$

where the optical depth function  $\kappa(\eta_0, \eta)$  is related to the differential optical depth  $q(\eta)$  by  $q(\eta) = -d\kappa(\eta_0, \eta)/d\eta$ . Fig.3 shows the profile of  $V(\eta)$  from the numerical result by cmbfast, which is sharply peaked around the last scattering. In practical calculation it is usually fitted by a narrow Gaussian form [24, 26]

$$V(\eta) = V(\eta_d) \exp\left(-\frac{(\eta - \eta_d)^2}{2\Delta\eta_d^2}\right), \quad (45)$$

where  $V(\eta_d)$  is the amplitude at the the decoupling time  $\eta_d$ , and  $\Delta\eta_d$  is the thickness of decoupling. The analysis of the WMAP data [3] gives the redshift thickness of the decoupling  $\Delta z_d = 195 \pm 2$ , which corresponds to  $\Delta\eta_d/\eta_0 = 0.00143$ . Then, taking  $V(\eta_d)\eta_0 = 279$  and in (45) yields a fitting shown in Fig.3, which has large error on both side of  $\eta_d$ , compared with the numerical one. To improve the fitting of  $V(\eta)$ , we take the following analytic expressions, which consists of two half-gaussian functions,

$$V(\eta) = V(\eta_d) \exp\left(-\frac{(\eta - \eta_d)^2}{2\Delta\eta_{d1}^2}\right), \quad (\eta < \eta_d); \quad (46)$$

$$V(\eta) = V(\eta_d) \exp\left(-\frac{(\eta - \eta_d)^2}{2\Delta\eta_{d2}^2}\right), \quad (\eta > \eta_d); \quad (47)$$

with  $\Delta\eta_{d1}/\eta_0 = 0.00110$ ,  $\Delta\eta_{d2}/\eta_0 = 0.00176$ , and  $(\Delta\eta_{d1} + \Delta\eta_{d2})/2 = \Delta\eta_d$ , satisfying the constraint of (44). Fig.3 shows that the half-gaussian model fits the numerical one much better than the Gaussian fitting, especially, on the left-hand side of the peak the area enclosed between the curves of the Gaussian and the half-gaussian is about  $\sim 11\%$  of the total area enclosed under the curve  $V(\eta)$ . As shall be seen later, this difference in  $V(\eta)$  will subsequently cause a variation in the hight of the polarization spectrum. The expressions (46) and (47) will be used to calculate the approximate analytic polarization power spectrum, which turns out to depend more sensitively on the smaller time interval  $\Delta\eta_{d1}$ .

## 6. Analytic Solution.

We start to look for the analytic solution of Eqs.(10) and (11). Since the blackbody spectrum  $f(\nu_0)$  in the Rayleigh-Jeans zone has the property  $\frac{d \ln f_0(\nu_0)}{d \ln \nu_0} \approx 1$ , these equations reduce to

$$\dot{\xi} + [ik\mu + q]\xi = \dot{h}, \quad (48)$$

$$\dot{\beta} + [ik\mu + q]\beta = \frac{3q}{16} \int_{-1}^1 d\mu' \left[ (1 + \mu'^2)^2 \beta - \frac{1}{2}(1 - \mu'^2)^2 \xi \right]. \quad (49)$$

In Eq.(48) the GW  $\dot{h}$  play the role of source for the anisotropies  $\xi$ , while the term  $q\xi$  causes  $\xi$  to damp. The formal solution of Eq.(48) is

$$\xi(\eta) = \int_0^\eta \dot{h}(\eta') e^{-\kappa(\eta, \eta')} e^{ik\mu(\eta' - \eta)} d\eta'. \quad (50)$$

In Eq.(49) the integration over  $\mu$  contains the functions  $\beta$  and  $\xi$ . Using  $\xi_l$  and  $\beta_l$  defined in Eqs.(15) and (14), then Eq.(49) is

$$\dot{\beta} + [ik\mu + q]\beta = qG, \quad (51)$$

where

$$G(\eta) \equiv \frac{3}{35}\beta_4 + \frac{5}{7}\beta_2 + \frac{7}{10}\beta_0 - \frac{3}{70}\xi_4 + \frac{1}{7}\xi_2 - \frac{1}{10}\xi_0.$$

One might write down a formal solution

$$\beta(\eta) = \int_0^\eta G(\eta') q(\eta') e^{-\kappa(\eta, \eta')} e^{ik\mu(\eta' - \eta)} d\eta', \quad (52)$$

and set the the time  $\eta$  in the above to be the present time  $\eta_0$ ,

$$\beta(\eta_0) = \int_0^{\eta_0} G(\eta') V(\eta') e^{ik\mu(\eta' - \eta_0)} d\eta', \quad (53)$$

where  $V(\eta') = q(\eta') e^{-\kappa(\eta_0, \eta')}$  is the visibility function. However, the difficulty with the integration (53) is that the integrand  $G$  contains  $\beta_l$  and  $\xi_l$  up to  $l = 4$ , which are not known yet.

One uses the Legendre expansion and write Eqs.(48) and (49) as the following hierarchical set of equations:

$$\dot{\xi}_0 = -q\xi_0 - ik\xi_1 + \dot{h}, \quad (54)$$

$$\dot{\beta}_0 = -\frac{3}{10}q\beta_0 - ik\beta_1 + q \left( \frac{3}{35}\beta_4 + \frac{5}{7}\beta_2 - \frac{3}{70}\xi_4 + \frac{1}{7}\xi_2 - \frac{1}{10}\xi_0 \right), \quad (55)$$

$$\dot{\xi}_l = -q\xi_l - \frac{ik}{2l+1} [l\xi_{l-1} + (l+1)\xi_{l+1}], \quad \text{for } l \geq 1, \quad (56)$$

$$\dot{\beta}_l = -q\beta_l - \frac{ik}{2l+1} [l\beta_{l-1} + (l+1)\beta_{l+1}], \quad \text{for } l \geq 1. \quad (57)$$

In the tight coupling limit with  $q \rightarrow \infty$ , the equations reduce to

$$\dot{\xi}_0 + q\xi_0 = \dot{h}, \quad (58)$$

$$\dot{\beta}_0 + \frac{3}{10}q\beta_0 = -\frac{1}{10}q\xi_0, \quad (59)$$

$$\xi_l = \beta_l = 0, \quad l \geq 1. \quad (60)$$

Then the source function  $G(\eta)$  reduces to  $G = (7\beta_0 - \xi_0)/10$ , and satisfies the equation:

$$\dot{G} + \frac{3}{10}qG = -\frac{1}{10}\dot{h}, \quad (61)$$

and the formal solution is

$$G(\eta) = -\frac{1}{10} \int_0^\eta \dot{h}(\eta'') e^{-\frac{3}{10}\kappa(\eta, \eta'')} d\eta''. \quad (62)$$

Substitute this expression of  $G$  into Eq.(53), yields the formal solution for the polarization in the tight coupling limit:

$$\begin{aligned} \beta(\eta_0) &= \int_0^{\eta_0} V(\eta') \left[ -\frac{1}{10} \int_0^{\eta'} \dot{h}(\eta'') e^{-\frac{3}{10}\kappa(\eta', \eta'')} d\eta'' \right] e^{ik\mu(\eta' - \eta_0)} d\eta' \\ &= -\frac{1}{10} \int_0^{\eta_0} d\eta' V(\eta') e^{ik\mu(\eta' - \eta_0)} \int_0^{\eta'} d\eta'' \dot{h}(\eta'') e^{-\frac{3}{10}\kappa(\eta'') + \frac{3}{10}\kappa(\eta')}, \end{aligned} \quad (63)$$

where  $\kappa(\eta) \equiv \kappa(\eta_0, \eta)$ .

Note that this approximate result of the tight coupling applies only on scales much larger than the mean free path of photons. On smaller scales the effects of photon diffusion will cause some damping in the anisotropy and polarization. To take care of this effect, we now expand Eqs.(54)-(57) to the second order of the small parameter  $1/q \ll 1$ , which has the meaning of the mean free path, and arrive at,

$$\dot{\xi}_0 = -q\xi_0 - ik\xi_1 + \dot{h}, \quad (64)$$

$$\dot{\xi}_1 = -q\xi_1 - \frac{ik}{3}\xi_0, \quad (65)$$

$$\xi_l = 0, \quad l \geq 2. \quad (66)$$

Putting  $\xi_0 \propto e^{i \int \omega d\eta}$  and  $\xi_1 \propto e^{i \int \omega d\eta}$  and substituting into Eqs.(64) and (65), ignoring variations of  $\omega$  on the expansion scale  $\dot{a}/a$ , neglecting  $\dot{h}$  which is nearly zero at low frequency, shown in Fig.2, one gets

$$\omega = \pm \frac{k}{\sqrt{3}} + iq.$$

Thus  $\xi_0$  will acquire an extra damping factor  $e^{-\int q d\eta}$ , independent on the wavenumber  $k$ . This feature is different from the case of the scalar perturbations, where the damping is strong on the small scales [43]. For the polarization  $\beta$ , we only keep the tight coupling limit with the equation,

$$\dot{\beta}_0 = -\frac{3q}{10}\beta_0 - \frac{q}{10}\xi_0,$$

which follows that  $\beta_0$  also gets a damping of  $e^{-\int q d\eta}$ . Thus, taking into the account of the diffusion effect,  $G$  in (62) will acquire an extra damping factor  $\exp(-\kappa(\eta))$ , and (63) becomes

$$\beta(\eta_0) = -\frac{1}{10} \int_0^{\eta_0} d\eta' V(\eta') e^{ik\mu(\eta' - \eta_0)} \int_0^{\eta'} d\eta'' \dot{h}(\eta'') e^{-\frac{3}{10}\kappa(\eta'') - \frac{7}{10}\kappa(\eta')}. \quad (67)$$

In the above the function  $\exp(-\frac{3}{10}\kappa(\eta'')) \simeq 0$  for  $\eta < \eta_d$ , and  $\exp(-\frac{3}{10}\kappa(\eta'')) \simeq 1$  for  $\eta > \eta_d$ , so it can be approximated as a step function  $\exp(-\frac{3}{10}\kappa(\eta'')) \approx \theta(\eta'' - \eta_d)$ , and

moreover, the visibility function  $V(\eta')$  is also peaked about the decoupling  $\eta_d$ . Therefore, as an approximation, one can pull the  $\dot{h}(\eta'')$  out of the integration  $\int d\eta''$ ,

$$\beta(\eta_0) = -\frac{1}{10} \int_0^{\eta_0} d\eta V(\eta) e^{ik\mu(\eta-\eta_0)} \dot{h}(\eta) \int_0^\eta d\eta' e^{-\frac{3}{10}\kappa(\eta') - \frac{7}{10}\kappa(\eta)}. \quad (68)$$

Define the integration variable  $x \equiv \kappa(\eta')/\kappa(\eta)$  to replace the variable  $\eta'$ . For  $V(\eta)$  is peaked around the  $\eta_d$  with width  $\Delta\eta_d$ , one can take  $d\eta' = \frac{dx}{x} \Delta\eta_d$  as an approximation, then

$$\beta(\eta_0) = -\frac{1}{10} \Delta\eta_d \int_0^{\eta_0} d\eta V(\eta) e^{ik\mu(\eta-\eta_0)} \dot{h}(\eta) \int_1^\infty \frac{dx}{x} e^{-\frac{3}{10}\kappa(\eta)x} e^{-\frac{7}{10}\kappa(\eta)}, \quad (69)$$

Substituting this into Eq.(15) and using the expansion formula

$$e^{ikr \cos \theta} = \sum_{l=0}^{\infty} (2l+1) i^l j_l(kr) P_l(\cos \theta),$$

one arrives at the expression for the component of the polarization

$$\beta_l(\eta_0) = -\frac{1}{10} \Delta\eta_d i^l \int_0^{\eta_0} d\eta V(\eta) \dot{h}(\eta) j_l(k(\eta - \eta_0)) \int_1^\infty \frac{dx}{x} e^{-\frac{3}{10}\kappa(\eta)x} e^{-\frac{7}{10}\kappa(\eta)}. \quad (70)$$

Now look at the integration  $\int d\eta$  involving  $V(\eta)$ , which has a factor of the form  $e^{-a(\eta-\eta_d)^2}$ . As a stochastic quantity, the time-derivative of GW  $\dot{h}(\eta)$  contains generally a mixture of oscillating modes, such as  $e^{ik\eta}$  and  $e^{-ik\eta}$ , and so does the spherical Bessel function  $j_l(k(\eta - \eta_0))$ . Thus  $\dot{h}(\eta) j_l(k(\eta - \eta_0))$  generally contains terms  $\propto e^{-ibk(\eta-\eta_0)}$ , where  $b \in [-2, 2]$ . Using the formula

$$\int_{-\infty}^{\infty} e^{-ay^2} e^{ibky} dy = e^{-\frac{(bk)^2}{4a}} \int_{-\infty}^{\infty} e^{-ay^2} dy,$$

the integration is approximately

$$\int_0^{\eta_0} d\eta V(\eta) \dot{h}(\eta) j_l(k(\eta - \eta_0)) \approx e^{-\alpha(k\Delta\eta_d)^2} \dot{h}(\eta_d) j_l(k(\eta_d - \eta_0)) \int_0^{\eta_0} d\eta V(\eta). \quad (71)$$

When the half-gaussian visibility function  $V(\eta)$  of Eq.(46) and (47) is used, the integration is approximated by

$$\int_0^{\eta_0} d\eta V(\eta) \dot{h}(\eta) j_l(k(\eta - \eta_0)) \approx \frac{1}{2} \left[ e^{-\alpha(k\Delta\eta_{d1})^2} + e^{-\alpha(k\Delta\eta_{d2})^2} \right] \dot{h}(\eta_d) j_l(k(\eta_d - \eta_0)) \int_0^{\eta_0} d\eta V(\eta). \quad (72)$$

In the above  $\alpha$  can take values in  $[0, 2]$ , depending on the phase of  $\dot{h}(\eta) j_l(k(\eta - \eta_0))$ . Here we will take  $\alpha$  as a parameter. This gives another damping depending on both  $\Delta\eta_d$  and  $k$ . This damping of the anisotropies  $\xi$  and  $\beta$  of CMB is caused by Thompson scattering of photons by free electrons. During the recombination around the last scattering, the visibility function  $V$  is narrowly centered around the the time  $\eta_d$  with a width  $\Delta\eta_d$ , so the smoothing by Thompson scattering is effectively limited within the interval  $\Delta\eta_d$ . Thus a wave of anisotropies  $e^{ik\eta}$  will be damped in this interval by an factor  $e^{-(k\Delta\eta_d)^2}$ . The longer the interval  $\Delta\eta_d$  is, the more damping the wave suffers. In fact  $\Delta\eta_d$  can be viewed as the thickness of the last scattering surface. Those waves with wavelength  $\lambda$  shorter than  $\Delta\eta_d$  will be effectively damped by a factor  $e^{-(2\pi\Delta\eta_d/\lambda)^2}$ , the same as before. Thus the shorter the wave length is, the more damping for the wave.

The remaining integrations in  $\beta_l$  is

$$\int_0^{\eta_0} d\eta V(\eta) \int_1^\infty \frac{dx}{x} e^{-\frac{3}{10}\kappa(\eta)x} e^{-\frac{7}{10}\kappa(\eta)} = \int_0^\infty d\kappa e^{-\frac{17}{10}\kappa} \int_1^\infty \frac{dx}{x} e^{-\frac{3}{10}\kappa x} = \frac{10}{17} \ln \frac{20}{3}. \quad (73)$$

We like to point out that this amplitude is the outcome from the second order of the tight-coupling limit, while the first order of the tight-coupling limit with  $G$  being given in (62) would yield a result  $\frac{10}{7} \ln \frac{10}{3}$  in Ref.[26]. Thus finally (70) yields

$$\beta_l(\eta_0) = -\frac{1}{17} \ln \frac{20}{3} i^l \Delta \eta_d \dot{h}(\eta_d) j_l(k(\eta_d - \eta_0)) D(k), \quad (74)$$

where

$$D(k) \equiv \frac{1}{2} \left[ e^{-\alpha(k\Delta\eta_{d1})^2} + e^{-\alpha(k\Delta\eta_{d2})^2} \right]. \quad (75)$$

for the half-gaussian visibility function. For the gaussian visibility function one would have  $D(k) \equiv e^{-\alpha(k\Delta\eta_d)^2}$ .

Substituting this back into Eqs.(28) and (29) yields the polarization spectra

$$C_l^{XX} = \frac{1}{16\pi} \left( \frac{1}{17} \ln \frac{20}{3} \right)^2 \int P_{Xl}^2(k(\eta_d - \eta_0)) |\dot{h}(\eta_d)|^2 \Delta \eta_d^2 D^2(k) k^2 dk, \quad (76)$$

where "X" denotes "G" or "C", the type of of the CMB polarization, for the electric type

$$P_{Gl}(x) = \frac{(l+2)(l+1)}{(2l-1)(2l+1)} j_{l-2}(x) - \frac{6(l-1)(l+2)}{(2l-1)(2l+3)} j_l(x) + \frac{l(l-1)}{(2l+3)(2l+1)} j_{l+2}(x), \quad (77)$$

and for the magnetic type

$$P_{Cl}(x) = \frac{2(l+2)}{2l+1} j_{l-1}(x) - \frac{2(l-2)}{2l+1} j_{l+1}(x). \quad (78)$$

The result (76) is similar to the result in Ref.[26] (realizing that our  $(2\pi)^3$  Fourier conventions differ from theirs) if we identify  $C_l^{GG} = C_{El}/2$  and  $C_l^{CC} = C_{Bl}/2$ , but here the coefficient is  $\frac{1}{17} \ln \frac{20}{3}$ , smaller than that in Ref.[26] since we have also included the diffusion effect on the source  $\dot{G}$ . So the the second order of the tight-coupling limit reduces the amplitude by about  $\sim 58\%$ . Another difference is the damping factor  $D(k)$ . Besides, the parameter  $\alpha$  is taken to be in the range  $[0, 2]$ , instead of a fixed  $\alpha = 1/2$  as in Ref.[26].

To completely determine  $C_l^{XX}$ , we need to fix the normalization of the initial amplitude  $\dot{h}(\eta_d)$  in Eq.(76). What has been observed is the CMB temperature anisotropies, which generally has contributions from both the scalar and tensor perturbations. The ratio of the contributions

$$r = \frac{P_h(k_0)}{P_R(k_0)} \quad (79)$$

has not been fixed observationally, and only constraints can be given. Based upon the observations of Ly- $\alpha$  forest power spectrum from the SDSS, 3-year WMAP, supernovae and galaxy clustering, one can give a constraint of  $r < 0.22$  at 95% C.L. ( $< 0.37$ , at 99.9% C.L.) [44]. We take it as a parameter. WMAP observation [4] gives the scalar perturbation power spectrum

$$P_R(k_0) = 2.95 \times 10^{-9} A(k_0), \quad (80)$$

with  $k_0 = 0.05 \text{Mpc}^{-1}$  and the amplitude  $A(k_0) = 0.8$ . Taking the scale-invariant spectrum with  $n_T = 0$  in (33), then the amplitude  $A_T$  in (33) depends on  $r$ . For instance, if  $r = 1$  is taken, then  $A_T = 2.46 \times 10^{-9}$ , and smaller  $r$  will yield smaller  $A_T$  accordingly.

## 7. Results and Discussions

### *Damping Effects due to Visibility Function:*

The power spectra of  $C_l^{GG}$  and  $C_l^{CC}$ , calculated from our analytic formulae (76) and from the numerical cmbfast, have been shown in Figs.4 and 5, respectively. The approximate analytic result is quite close to the numerical one evaluated from the cmbfast code, especially, for the first three peaks of the spectrum that are observable. One sees that  $C_l^{GG}$  and  $C_l^{CC}$  at large  $l$  sensitively depend on the visibility function  $V$ , that is, on the factor  $D(k)$ . In particular for the electric polarization spectrum, our half-gaussian model  $D(k)$  in (75) with  $\alpha = 1.7$  gives very good fitting with the third peak being very close to the numerical one, and the second peak being higher. For  $\alpha = 2$  the second peaks of the spectra are good, but the third peaks are a bit too low. On the other hand, the Gaussian model  $D(k) = e^{-\alpha(k\Delta\eta_d)^2}$  with  $\alpha = 2$  yields a power spectrum too low. The reason is for  $\Delta\eta_d > \Delta\eta_{d1}$ . The larger value of  $\alpha$ , the larger damping of the power spectrum on the small scale.

### *The height of the power spectrums:*

Eq. (76) shows that the height of  $C_l^{XX}$  depends on the amplitude  $|\dot{h}(\eta_d)|$  at the decoupling time. As has been discussed earlier, for the scale-invariant power spectrum  $n_T \simeq 0$ ,  $|\dot{h}(\eta_d)|$  is directly related to the tensor-scalar ratio  $r$  in Eq.(79). A larger  $r$  yields a larger  $|\dot{h}(\eta_d)|$  and a higher polarization. Currently the observations have only given an upper limit of  $r < 0.22$  (95% C.L.) [44]. In Fig.6 we have plotted the analytic formula (76) for  $C_l^{CC}$ , for three values  $r = 0.3, 0.1, 0.01$ , respectively, whereby also plotted are the one-sigma sensitivity estimates of the near-term projects, WMAP and Planck satellites [45, 46, 47]. The WMAP estimates are based on measured noise properties of the instrument for an 8-year of operation, and the Planck estimates are based on noise measurements from the test-bed High Frequency Instrument for a 1.2-year of operation. Fig.6 clearly shows that the magnetic polarization for the models with  $r > 0.1$  can be detected by the Planck, but difficult for the WMAP.

However, in this discussion, we have not considered the effect of cosmic reionization process, which is directly related to the galaxy formation. The recent WMAP result [5] tends to give the optical depth of reionization  $\kappa_r = 0.09 \pm 0.03$ . Thus the visibility function  $V(\eta)$  will have another peak around the late time  $\eta/\eta_0 \sim 0.27$  besides the cosmic decoupling, and will give an extra contribution to  $C_l^{CC}$ , correspondingly. At present, the reionization process is not well understood yet, and it is difficult to give an analytic formula for this process. Using the numerical cmbfast including the reionization effect, we have plotted  $C_l^{CC}$  in Fig.7, where an extra peak of  $C_l^{CC}$  at  $l \sim 6$  is seen. On the observational side, a number of other projects are currently underway, such as CBI[48], DASI[49], CAPMAP[50], BOOMERANG[51], emphasizing on the CMB magnetic polarization. The future projects CLOVER[52] and QUIET[53] are expected to detect the magnetic polarization for  $r > 0.01$ , and the project CMBPOL [54] even for  $r > 10^{-3}$ .

### *The influence of width of decoupling:*

Besides the gravitational waves,  $C_l^{XX}$  also directly depend on the thickness of the decoupling  $\Delta\eta_d$ , and on the damping function  $D(k)$ . A smaller  $\Delta\eta_d$  makes the power spectrum having smaller height. This effect is obvious at the large scale (small  $l$ ). At the small scale (large  $l$ ), the effect is complicate since both  $\Delta\eta_d$  and the damping factor  $D(k)$  will influence the spectrum. The expression of  $D(k)$  shows that, for a fixed  $k$ , the smaller  $\Delta\eta_d$  leads to larger  $D(k)$ . The thickness of the decoupling is mainly determined by the baryon density  $\Omega_b$  of the Universe. In the flat  $\Lambda$ CDM Universe, increasing  $\Omega_b$  will slightly enhance the decoupling speed,

which will make  $\Delta\eta_d$  becoming smaller [42]. For example, a fitting formula can be used for the optical depth function in the  $\Lambda$ CDM Universe [23]

$$\kappa(z_0, z) = \Omega_b^{c_1} \left( \frac{z}{1000} \right)^{c_2}, \quad 800 < z < 1200, \quad (81)$$

where  $c_1 = 0.43$  and  $c_2 = 16 + 1.8 \ln \Omega_b$ . This function is only dependent on  $\Omega_b$ . The visibility function  $V(\eta) = \frac{dk}{d\eta} e^{-\kappa}$  is peaked around at  $\eta_d$ . A larger  $\Omega_b$  corresponds to a narrower  $V$  and smaller  $\Delta\eta_d$ , as shown in Fig.8, where three models  $\Omega_b = 0.02, 0.044, 0.09$  are given. Therefore, a higher  $\Omega_b$  leads to a lower  $C_l^{CC}$ , as shown in Fig.9 for these three values of  $\Omega_b$ .

*The location of the peaks:*

From the formula (76), we also can analyze the peak's location of the power spectrums. The factor functions  $P_{Gl}^2[k(\eta_d - \eta_0)]$  in (77) and  $P_{Cl}^2[k(\eta_d - \eta_0)]$  in (78) are all combination of the spherical Bessel function  $j_l(k(\eta_d - \eta_0))$ , which is peaked at  $l \simeq k(\eta_0 - \eta_d) \simeq k\eta_0$  for  $l \gg 1$ . In Fig.10 and Fig.11  $P_{Gl}$  and  $P_{Cl}$  are plotted with  $l = 100$ , where it is shown that  $P_{Gl}$  peaks at  $k\eta_0 \simeq l$ , and  $P_{Cl}$  peaks at  $k\eta_0 \simeq 1.27l$ . So the peak location of the power spectrums are directly determined by

$$C_l^{XX} \propto \left| \dot{h}(\eta_d) \right|^2 k^2 D^2(k) |_{k=l/\eta_0}, \quad (82)$$

The factor  $D(k)$  has a larger damping at larger  $l$ , so the first peak of the power spectrum has the highest amplitude. Let us look at the first peak of  $C_l^{XX}$ , where  $D(k) \simeq 1$ . Eq.(37) gives  $\dot{h}(\eta_d)^2 = A_0^2 k^2 (\eta_e/\eta_d)^2 [A_1 j_2(k\eta_d) + A_2 y_2(k\eta_d)]^2$ . Since  $j_2(k\eta_d)$  term is the increasing mode and the  $y_2(k\eta_d)$  term is the damping mode for the waves inside the horizon, so we can take  $\dot{h}(\eta_d)^2 \sim A_0^2 k^2 (\eta_e/\eta_d)^2 [A_1 j_2(k\eta_d)]^2$ . As  $j_2(x)$  peaks at nearly  $x \simeq 3$ , so  $\dot{h}(\eta_d)^2$  peaks at  $k\eta_d \simeq 3$ . Thus  $C_l^{XX}$  peaks around

$$l \simeq k\eta_0 \simeq 3\eta_0/\eta_d. \quad (83)$$

This sudden-change approximation is a reasonably good estimate. If we use the WKB approximation in the  $\Lambda$ CDM Universe with  $\eta_d/\eta_0 = 0.0195$ , then we find that the factor function  $\dot{h}(\eta_d)^2 k^2$  in Eq.(82) is peaked around  $k\eta_0 \sim 127$ , shown in Fig.12, while the sudden-change approximation in Eq.(83) gives  $k\eta_0 \sim 154$ . Therefore, the estimate (83) holds approximately. The value of  $\eta_0/\eta_d$  is related to the dark energy component and baryon component. For instance, we take the three models with  $\Omega_\Lambda = 0.65, 0.73$ , and  $0.80$ , respectively, and with fixed  $\Omega_b = 0.044$ ,  $\Omega_{dm} = 1 - \Omega_\Lambda - \Omega_b$ . Then a numerical calculation yields that  $\eta_0/\eta_d \simeq 50.1, 51.3$ , and  $53.6$ , respectively. The gravitational waves  $\dot{h}(\eta_d)$  also depends on  $\Omega_\Lambda$ , as shown in Fig.13, where it is clearly shown that a smaller  $\Omega_\Lambda$  will shift the peaks  $\dot{h}(\eta_d)$  slightly to larger scales. Correspondingly, a smaller  $\Omega_\Lambda$  will shift the peak of  $C_l^{XX}$  to larger scales, as demonstrated in Fig.14. So we have the conclusion that a lower dark energy  $\Omega_\Lambda$  makes the peak of  $C_l^{XX}$  to locate at smaller  $l$ . This suggests a new way to study the cosmic dark energy.

The baryon component also influence the decoupling time  $\eta_d$ . A larger  $\Omega_b$  has a larger decoupling time  $\eta_d$ , and therefore, a smaller  $l \simeq 3\eta_0/\eta_d$ . For fixed  $\Omega_\Lambda = 0.73$  and  $\Omega_{dm} = 1 - \Omega_\Lambda - \Omega_b$ , the three models with  $\Omega_b = 0.02, 0.044$ , and  $0.09$ , respectively, are given in Fig.8. The corresponding values are  $\eta_0/\eta_d = 54.9, 51.3$ , and  $50.1$ , respectively. So we have the conclusion that a higher baryon density  $\Omega_b$  makes the peak to locate at smaller  $l$ , as is demonstrated in Fig.9.

*The influence of the spectrum index  $n_T$  of relic GW on  $C_l^{XX}$ :*

The initial condition in (32) of the the relic GW will influence the CMB polarization. Not only the value of initial amplitude  $h(0)$  but also the index  $n_T$  in (33) will determine  $C_l^{XX}$ . To

reveal how the index  $n_T$  changes the  $C_l^{CC}$ , we plot in Fig.15 three curves of  $C_l^{CC}$  for  $n_T = -0.1, 0.0$ , and  $0.1$ , respectively, where the parameters are taken:  $r = 1$ ,  $\alpha = 2$  in the half-gaussian model. Fig.15 shows clearly that a larger value of  $n_T$  produces a higher polarization spectrum  $C_l^{CC}$ . The reason for this feature is the following:  $C_l^{CC} \propto |\dot{h}(\eta_d)|^2$ , and  $|\dot{h}(\eta_d)|$  differs from 0 only at larger  $k\eta_0 > 50$ , as in Fig.2, and  $|\dot{h}(\eta_d)| \propto k|h(\eta_d)|$ . Since  $k^3|h(\eta_d)|^2 \propto k^{n_T}$ , so in the range of larger  $k$  a larger value  $n_T$  will give a larger  $|h(\eta_d)|^2$  and a larger  $C_l^{CC}$ . Similar behavior also occurs for the electric polarization  $C_l^{GG}$ .

## 8. Conclusion.

In this paper we have analytically calculated the polarization power spectrum of CMB generated by relic gravitational waves in the Polnarev's method. As an approximate analytic result, it is quite close to the numerical one evaluated from the cmbfast code, especially, for the first three peaks of the spectrum that are observable. We have arrived at the analytic polarization spectra  $C_l^{XX}$  with several improvements over the previous results.

1. The spectrum  $C_l^{XX}$  is proportional to the relic gravitational waves  $|\dot{h}(\eta_d)|^2$ , the value of which is taken from the WKB approximation in our treatment, which is good compared with the numerical results. When looking for the location of the peaks of  $C_l^{XX}$  analytically, we find that it is very convenient to employ the analytic exact solution  $|\dot{h}(\eta_d)|^2$  from the sudden-change approximation. For instance, the first peak is found to be located at  $l \simeq 3\eta_0/\eta_d$ . Moreover, it has the merit that the dependence on the dark energy  $\Omega_\Lambda$  and the baryon  $\Omega_b$ , through the decoupling time  $\eta_d$ , is also clearly demonstrated. Both lower dark energy  $\Omega_\Lambda$  and higher baryon density  $\Omega_b$  make the peak of  $C_l^{XX}$  to locate at smaller  $l$ .

2. The visibility function describing the decoupling process has been given by the analytic half-gaussian approximation, which fits analytically the actual decoupling process better than the usual Gaussian model. For example, the improvement of  $V(\eta)$  on the left side of  $\eta_d$  in the half-gaussian model is considerable, which is about  $\sim 11.5\%$ , and correspondingly, this also leads an improvement on the spectrum  $\Delta C_l^{XX}/C_l^{XX} \sim 30\%$  around the second and the third peaks. The time integration  $V(\eta)$  yields the damping factor  $D(k)$ , which contains a parameter  $\alpha$  in the range  $[0, 2]$ , coming from the phase of the product of the  $\dot{h}(\eta)$  and  $j_l(k(\eta - \eta_0))$ . In particular, our half-gaussian model with  $\alpha \in (1.7, 2.0)$  gives a reasonably good fitting to the first three peaks of the spectra  $C_l^{XX}$ .

3. In dealing with the Boltzmann equations analytically, we have worked up to the second order of the tight coupling limit, resulting in an amplitude of  $C_l^{XX}$  smaller than that in the usual first order by 58%.

5. We have studied the influence of the power spectrum index of the relic GW on the CMB polarization, and have found that a larger value of  $n_T$  produces higher polarization spectra  $C_l^{CC}$  and  $C_l^{GG}$ .

ACKNOWLEDGMENT: We acknowledge the using of CMBFAST program [21]. We thank J.R.Pritchard for helpful discussions. Y. Zhang's research work has been supported by the Chinese NSF (10173008), NKBRF (G19990754), and by SRFDP.

## References

- [1] C.L.Bennett, *et al.*, *Astrophys.J.Suppl.* **148** (2003) 1;
- [2] A.Kogut, *et al.*, *Astrophys.J.Suppl.* **148** (2003) 161;



- [3] D.N.Spergel, *et al.*, *Astrophys.J.Suppl.* **148** (2003) 175;
- [4] H.V.Peiris, *et al.*, *Astrophys.J.Suppl.* **148** (2003) 213;
- [5] D.N.Spergel, *et al.*, *arXiv:astro-ph/0603449*;
- [6] L.Page, *et al.*, *arXiv:astro-ph/0603450*;
- [7] S. Sasaki, *Prog.Theor.Phys.* **76** (1986) 1036;
- [8] E.W.Kolb and M.S.Turner, *The Early Universe*, Addison-Wesley Publishing Company (1990);
- [9] V.F.Mukhanov, H.A.Feldman, and R.H.Brandenberger, *Phys.Rept.* **215** (1992) 203 ;
- [10] V.A.Rubakov, M.Sazhin, and A.Veryaskin, *Phys.Lett.* **B115** (1982) 189;
- [11] R.Fabbri and M.D.Pollock, *Phys.Lett.* **B125** (1983) 445;
- [12] L.Abbott and M.Wise, *Nuc.Phys.* **B237** (1984) 226;
- [13] A.Starobinskii, *Sov.Astron.Lett.* **11** (1985) 133;
- [14] A.Polnarev, *Sov.Astron.* **29** (1985) 6;
- [15] R.Sunyaev and Y.Zeldovich, *Astrophys.Space Sci.* **7** (1970) 3;
- [16] P.J.E.Peebles and J.T.Yu, *Astrophys.J.* **162** (1970) 815;
- [17] LIGO Scientific Collaboration: B.Abbott *et al.*, *Phys.Rev.Lett.* **95** (2005) 221101;
- [18] <http://lisa.nasa.gov/>;
- [19] <http://universe.nasa.gov/program/bbo.html>;
- [20] N.Seto, S.Kawamura and T.Nakamura, *Phys.Rev.Lett.* **87** (2001) 221103;
- [21] U.Seljak and M.Zaldarriaga, *Astrophys.J.* **469** (1996) 437;
- [22] A.Lewis, A.Challinor and A.Lasenby, *Astrophys.J.* **538** (2000) 473;
- [23] W.Hu and N.Sugiyama, *Astrophys.J.* **444** (1995) 489;
- [24] M.Zaldarriaga and D.D.Harari, *Phys.Rev.D* **52** (1995) 3276;
- [25] L.P.Grishchuk *Phys.Rev.D* **48** (1993) 3513; *Phys.Rev.Lett.* **70** (1993) 2371;
- [26] J.R.Pritchard and M.Kamionkowski, *Annals Phys.* **318** (2005) 2;
- [27] D.Harari and M.Zaldarriaga, *Phys.Lett.B* **310** (1993) 96;
- [28] K.L.Ng and K.W.Ng, *Astrophys.J.* **445** (1995) 521;
- [29] A.Kosowsky, *Annals Phys.* **246** (1996) 49;
- [30] M.Kamionkowski, A.Kosowsky, A.Stebbins, *Phys.Rev.D* **55** (1997) 7368;
- [31] B.Keating, *et al.*, *Astrophys.J.* **495** (1998) 580;
- [32] P.Cabella and M.Kamionkowski, *arXiv:astro-ph/0403392*;
- [33] Y.Zhang, H.Hao and W.Zhao, *ChA&A*, **29** (2005) 250;
- [34] S.Chandrasekhar, *Radiative Transfer* (Dover, New York, 1960).
- [35] R.K.Sachs and A.M.Wolfe, *Astrophys.J.* **147** (1967) 73;
- [36] S.Weinberg, *Phys.Rev.D* **69** (2004) 023503;
- [37] D.A.Dicus and W.W.Repko, *Phys.Rev.D* **72** (2005) 088302;
- [38] L.P.Grishchuk *Sov.Phys.JETP*, **40** (1974) 49;
- [39] Y.Zhang *et al.* *Class.Quant.Grav.* **22** (2005) 1383; *Class.Quant.Grav.* **23** (2006) 3783;

- [40] K.Ng and A.Speliotopoulos, Phys.Rev.D**52** (1995) 4;
- [41] P.J.E.Peebles, Astrophys.J. **153** (1968) 1;
- [42] B.Jones and R.Wyse, A&A **149** (1985) 144;
- [43] W.Hu and N.Sugiyama, Astrophys.J. **471** (1996) 542;
- [44] U.Seljak, A.Slosar and P.McDonald, arXiv:astro-ph/0604335;
- [45] J.Bock, arXiv:astro-ph/0604101;
- [46] <http://map.gsfc.nasa.gov/>;
- [47] P.Collaboration, arXiv:astro-ph/0604069;
- [48] <http://www.astro.caltech.edu/~tjp/CBI/>;  
J.L.Sievers *et al.*, arXiv:astro-ph/0509203;
- [49] <http://astro.uchicago.edu/dasi/>;  
E.M.Leitch *et al.*, Astrophys.J. **624** (2005) 10;
- [50] <http://www.phy.princeton.edu/cosmology/capmap/>;  
D.Barkats *et al.*, Astrophys.J. **619** (2005) L127;
- [51] <http://cmb.phys.cwru.edu/boomerang/>;  
G.Polenta *et al.*, Adv.Space Res., **36** (2005) 1064;
- [52] <Http://www.mrao.cam.ac.uk/~act21/clover.html>  
A.C.Taylor, *et al.*, arXiv:astro-ph/0407148;
- [53] <http://quiet.uchicago.edu>.
- [54] <http://universe.nasa.gov/program/inflation.html>;  
L.Verde, H.Peiris and R.Jimenez, JCAP **0601** (2006) 019;

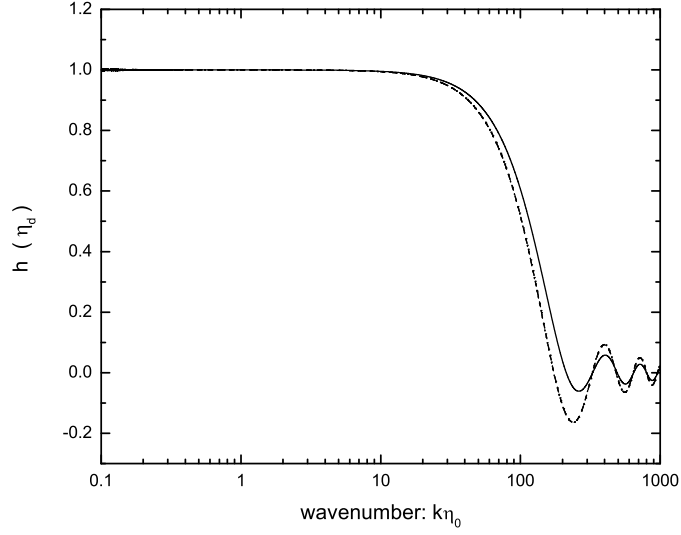


Figure 1: The gravitational waves  $h(\eta_d)$  depends on the scale factor  $a(\eta)$ . The solid line is the result of the sudden-change approximation, the dash line is the WKB approximation result, and the dot line is the numerical results, which is nearly overlapped with the dash line. Note that, here the initial gravitational waves have been rescaled with  $h(k) = 1$  for demonstrational purpose.

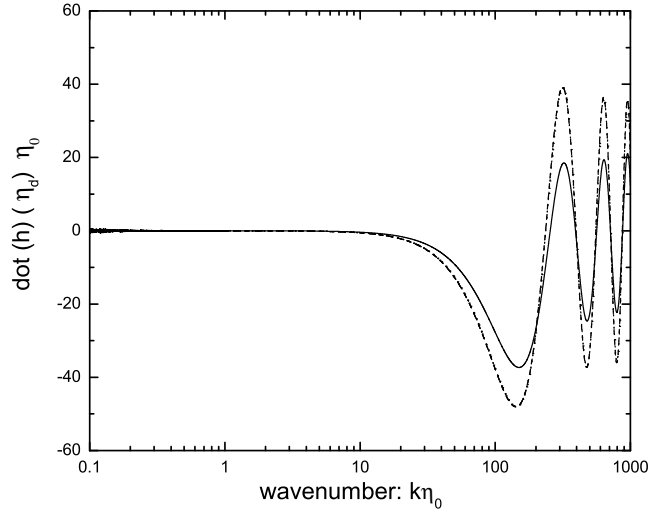


Figure 2: The gravitational waves  $\dot{h}(\eta_d)$  depends on the scale factor  $a(\eta)$ . The solid line is the result of the sudden-change approximation, the dash line is the WKB approximation result, and the dot line is the numerical results, which is nearly overlapped with the dash line. Again the rescaled  $h(k) = 1$  is used as in Fig.1.

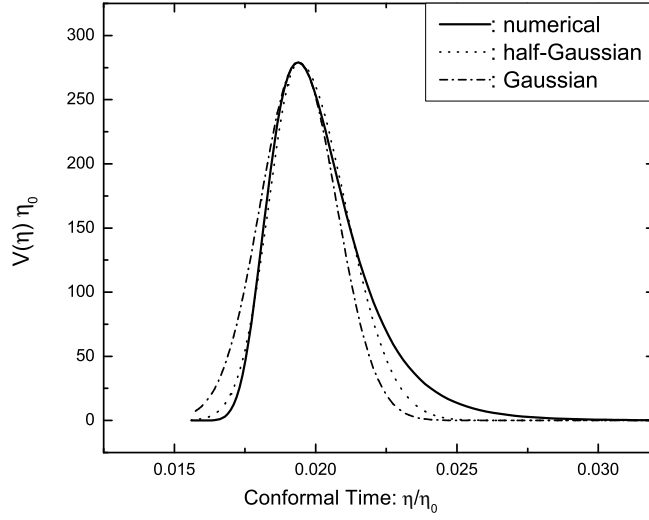


Figure 3: The visibility function  $V(\eta)$  around the decoupling. The solid line denotes the numerical result, the dash dot line denotes the gaussian fitting in Eq.(45) with  $\Delta\eta_d/\eta_0 = 0.00143$  and  $V(\eta_d)\eta_0 = 279$ , and the dot line denotes our half-gaussian fitting in Eqs.(46) and (47) with  $\Delta\eta_{d1}/\eta_0 = 0.00110$  and  $\Delta\eta_{d2}/\eta_0 = 0.00176$ . Here  $\eta_d/\eta_0 = 0.020$ . There is an area of strip on the left side of  $\eta_d$  in the Gaussian model differing from the numerical result, which is about  $\sim 11.5\%$ . This variation will lead to an error in the spectrum  $C_l^{XX}$  correspondingly.

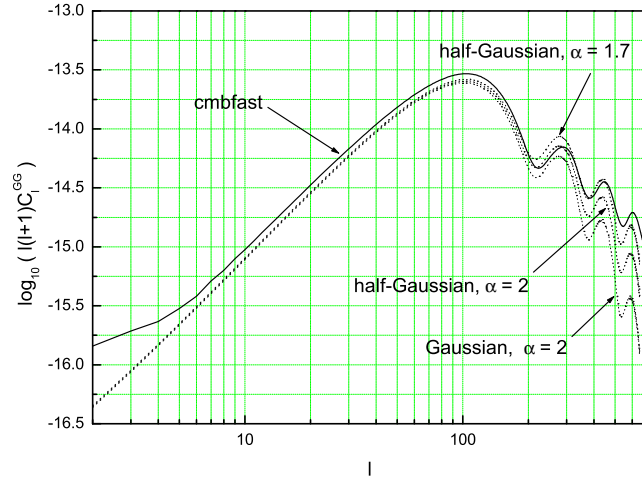


Figure 4: The “electric” polarization power spectrum  $C_l^{GG}$  with the ratio  $r = 1$ . The solid line denotes the numerical spectrum from CMBFAST code, and the dot lines denote the analytic results. The upper dot line is the result of the half-gaussian visibility function with  $\alpha = 1.7$ , the middle dot line is the result of the half-gaussian visibility function with  $\alpha = 2$  and, and the lower dot line is the result from the Gaussian visibility function with  $\alpha = 2$ . While at large scales these models are close to each other, the half-gaussian model improves the spectrum height of the 3<sup>rd</sup> peak by about  $\Delta \log_{10} C_l^{GG} \sim 0.2$ .

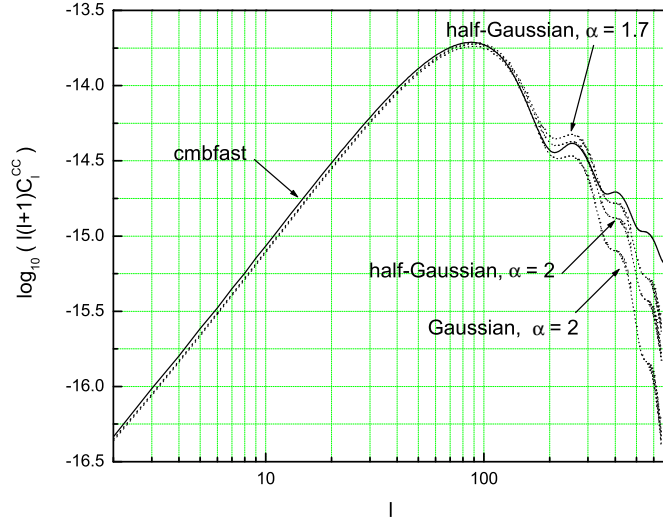


Figure 5: The “magnetic” polarization power spectrum  $C_l^{CC}$  with the ratio  $r = 1$ . The solid line denotes the numerical spectrum from CMBFAST code, and the dot lines denote the analytic results. The upper dot line is the result from the half-gaussian visibility function with  $\alpha = 1.7$ , the middle dot line is the result from the half-gaussian visibility function with  $\alpha = 2$ , and the lower one is the result from the Gaussian visibility function with  $\alpha = 2$ . Again at large scales these models are close to each other, but the half-gaussian model improves the spectrum height of the 2<sup>nd</sup> peak by about  $\Delta \log_{10} C_l^{CC} \sim 0.1$ .

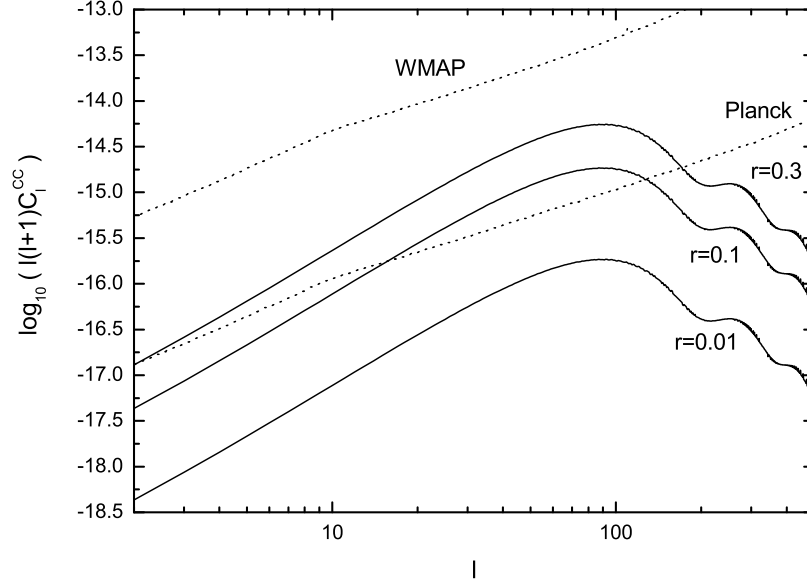


Figure 6: The WMAP and Planck satellite measurements on the CMB magnetic polarization signal. The three solid curves show the analytic polarization power spectra  $C_l^{CC}$  for the tensor-scalar ratio  $r = 0.3, 0.1, 0.01$ , respectively, in the  $\Lambda$ CDM Universe with  $\Omega_b = 0.044$ ,  $\Omega_{dm} = 0.226$ ,  $\Omega_\Lambda = 0.73$ .

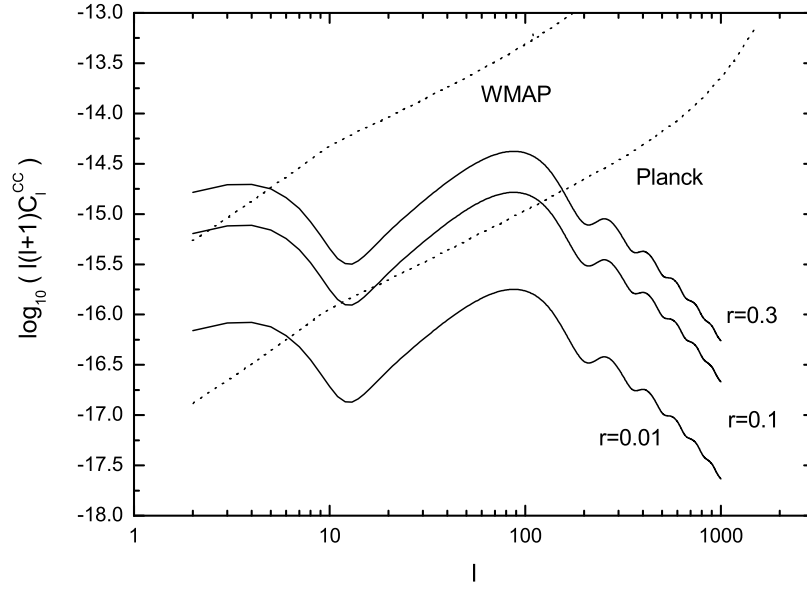


Figure 7: The WMAP and Planck satellite measurements on the CMB magnetic polarization signal. The parameters are the same as in Fig.6. The solid lines show the numerical  $C_l^{CC}$  using cmbfast. Here we have included the influence of cosmic reionization with the reionization optical depth  $\kappa_r = 0.09$ .

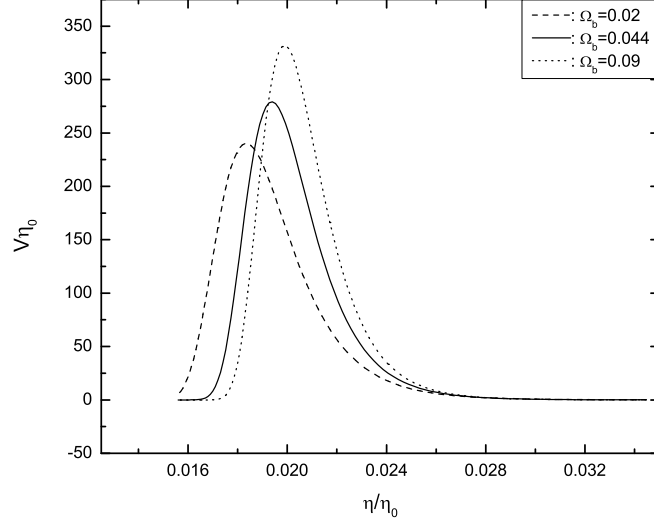


Figure 8: The dependence of the visibility function  $V(\eta)$  on the baryon  $\Omega_b$  in  $\Lambda$ CDM Universe with  $\Omega_\Lambda = 0.73$ , and  $\Omega_{dm} = 1 - \Omega_\Lambda - \Omega_b$ . The baryon density has been taken to be  $\Omega_b = 0.02, 0.044, 0.09$ , respectively.

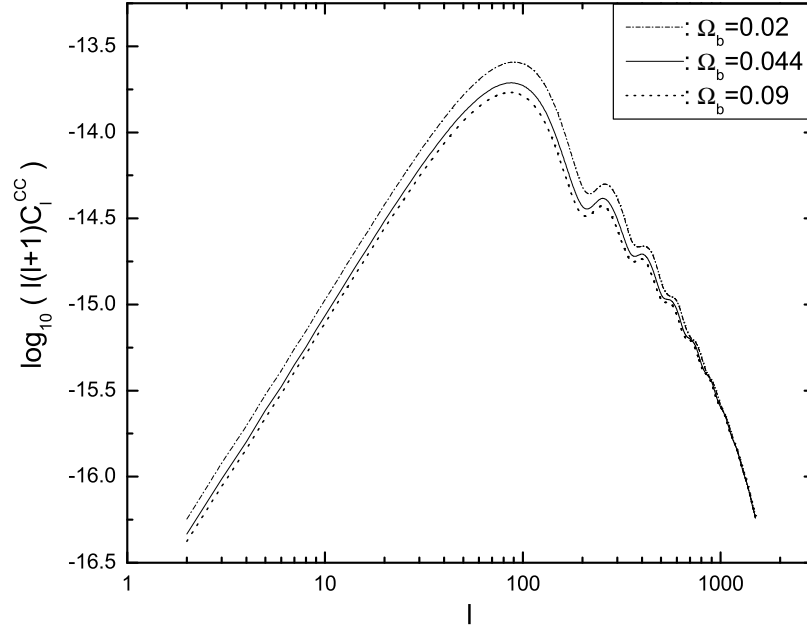


Figure 9: The dependence of the magnetic polarization power spectrums on the baryon  $\Omega_b$  in  $\Lambda$ CDM Universe with  $\Omega_\Lambda = 0.73$ ,  $\Omega_{dm} = 1 - \Omega_\Lambda - \Omega_b$ , and  $r = 1$ . The baryon  $\Omega_b = 0.02, 0.044, 0.09$ , has been taken respectively, as in Fig.8.



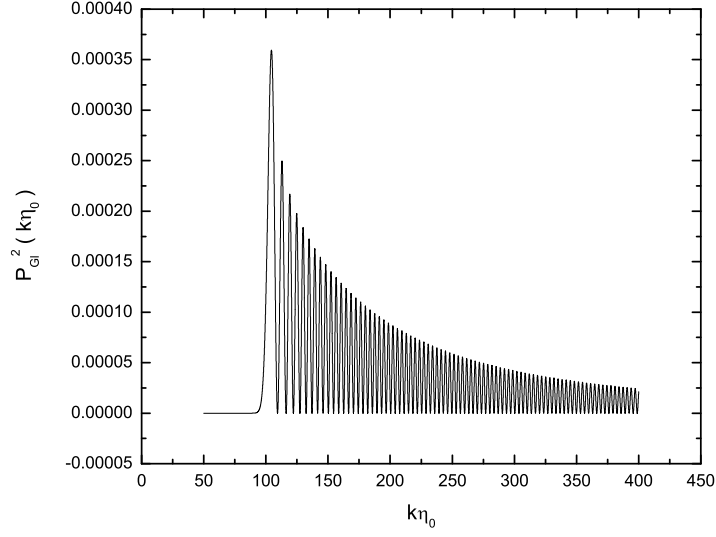


Figure 10: The factor  $P_{Gl}^2(k)$  as given in Eq.(77) with fixed  $l = 100$  as a function of the wave number  $k$ . Obviously it is peaked around  $k\eta_0 \sim 100$ , verifying the relation (83).

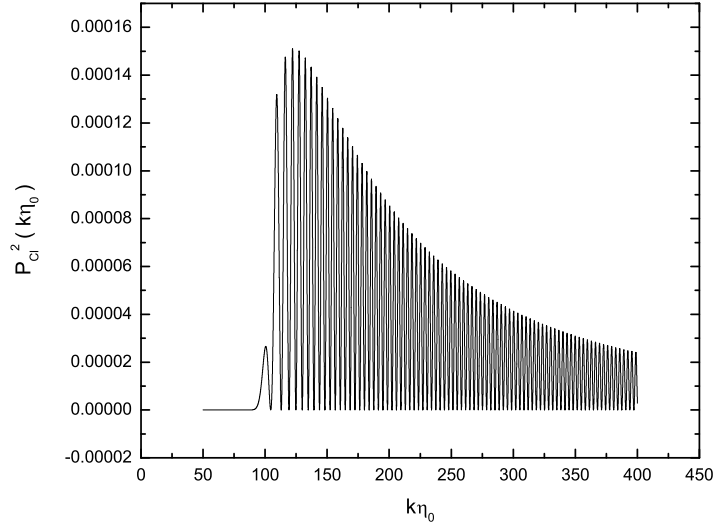


Figure 11: The factor  $P_{Cl}^2(k)$  as given in Eq.(78) with fixed  $l = 100$  as a function of the wave number  $k$ . It is approximately peaked around  $k\eta_0 \sim 127$ , thus (83) as an estimate holds approximately.

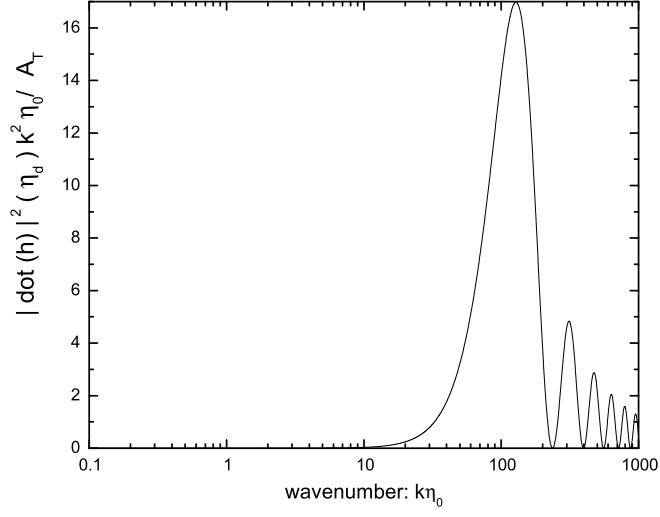


Figure 12: In the WKB approximation the factor function  $|\dot{h}(\eta_d)|^2 k^2 \eta_0 / A_T$  is peaked around  $\sim 127$ , validating the relation (83) as a fairly good estimate. Here the factor  $|\dot{h}(\eta_d)|^2 k^2$  is multiplied by a factor  $\eta_0 / A_T$  only for a clear graphical demonstration.

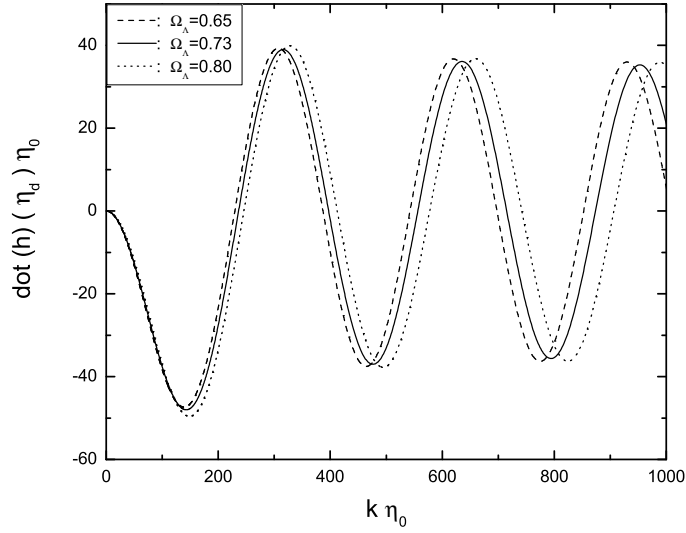


Figure 13: The influence of the dark energy  $\Omega_\Lambda$  on the time derivative of GW,  $\dot{h}(\eta_d)$ , at the decoupling. A larger value of  $\Omega_\Lambda$  shifts the peaks of  $\dot{h}(\eta_d)$  to smaller scales.

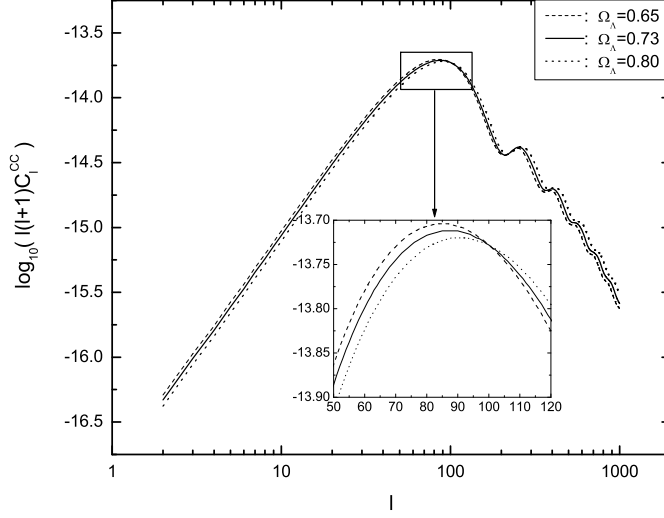


Figure 14: The magnetic polarization spectrum  $C_l^{CC}$  depends weakly on  $\Omega_\Lambda$ , and a larger value of  $\Omega_\Lambda$  shifts the peaks of slightly to smaller scales.

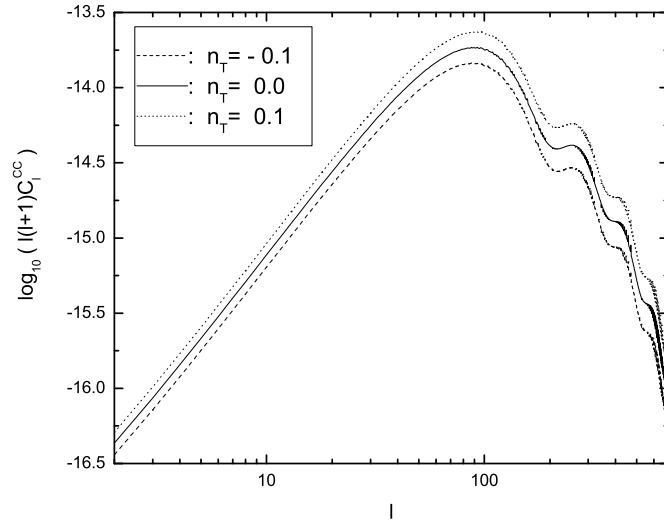


Figure 15: The magnetic polarization spectrum  $C_l^{CC}$  depends on the spectrum index  $n_T$  of the relic GW.  $C_l^{CC}$  are plotted for three values of  $n_T = -0.1, 0.0$ , and  $0.1$ , respectively. The following parameters are taken:  $r = 1$ ,  $\alpha = 2$  in the half-gaussian model. A larger value of  $n_T$  produces a higher spectrum  $C_l^{CC}$ .